CHEMISTRY OF MATERIALS
Cite This: Chem. Mater. XXXX, XXX, XXX−XXX
Article
pubs.acs.org/cm

Charge Transport in Alkali-Metal Superoxides: A Systematic First-Principles Study

Nicolai Rask Mathiesen,[#,¶] Sheng Yang,[†,¶] Juan Maria García-Lastra,[*,#] Tejs Vegge,[#] and Donald J. Siegel[*,‡,§,∥,⊥,#]

[†]Department of Physics, [‡]Mechanical Engineering Department, [§]Materials Science & Engineering, [∥]Applied Physics Program, and [⊥]University of Michigan Energy Institute, University of Michigan, Ann Arbor, Michigan 48109, United States

[#]Department of Energy Conversion and Storage, Technical University of Denmark, Fysikvej, Building 309, Kgs Lyngby 2800, Denmark

Supporting Information

ABSTRACT: Charge-transport mechanisms within the discharge products of alkali-metal/O_2 batteries can strongly influence the performance of these systems. To date, discharge products comprising alkali peroxides (Li_2O_2 and Na_2O_2) and superoxides (LiO_2, NaO_2, and KO_2) have been observed. In general, cells that discharge to a superoxide exhibit lower overpotentials than those that form the corresponding peroxide. These lower overpotentials have been hypothesized to originate from more efficient charge transport within the superoxides. While the transport mechanisms in the peroxides have been well studied, consensus regarding the intrinsic conductivity across the alkali-metal superoxides is lacking. Here, we present a systematic first-principles study of charge-transport mechanisms across the alkali-metal (Li, Na, K) superoxides. Our study draws on our prior investigations of the alkali peroxides and of sodium superoxide, while adding new analyses for lithium and potassium superoxides (LiO_2 and KO_2). In the case of KO_2, a nonsymmetrized room-temperature structure is proposed to account for a dynamic Jahn−Teller effect. Band gaps, equilibrium (charged) defect concentrations, mobilities, and intrinsic conductivities are estimated for both LiO_2 and KO_2. Overall, the alkali superoxides are predicted to be wide band gap insulators, with gaps exceeding 4 eV. These large band gaps imply that negligible transport occurs via band conduction. Compared to the alkali peroxides, ionic conductivities in the superoxides are predicted to be 8−11 orders of magnitude larger, ranging from 4×10^{-9} to 5×10^{-12} S/cm at room temperature. Regarding electronic conductivities, transport in NaO_2 and KO_2 is predicted to occur via polaron hopping, with low conductivities on the order of 10^{-19} to 10^{-20} S/cm. These values are similar to what has been previously reported for the peroxides. Importantly, the present calculations indicate that LiO_2 has a much larger electronic conductivity (also arising from polaron hopping) than its Na and K analogues, 9×10^{-12} S/cm at 300 K. These data suggest that the low overpotentials observed for Na- and KO_2-based batteries cannot be explained by high intrinsic electronic conductivities. In contrast, the much larger conductivities predicted for LiO_2 imply that the superior performance observed in LiO_2-based cells may reflect the ability of LiO_2 to support higher charge-transport rates.

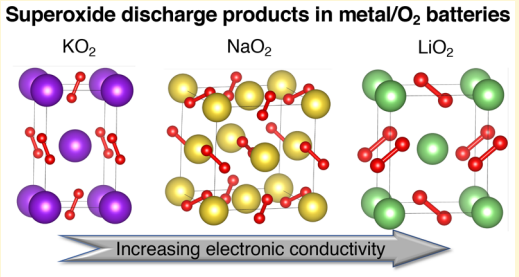

INTRODUCTION

Nonaqueous metal/oxygen batteries are intriguing next-generation energy storage devices, given their high theoretical specific energies and potential for rechargeability. However, many challenges remain to be overcome before these systems can realize their potential in a practical device.[1−8] Among these challenges is low cycling efficiency due to high overpotentials commonly observed during recharge.[4] High overpotentials can result from side reactions in the cathode, and from the often low intrinsic conductivity of the discharge product.[9−11] Adding to these challenges is the growing complexity of the experimental literature, which now contains reports of metal−oxygen batteries based on lithium,[4] sodium,[12] and potassium[6] negative electrodes.

Among the possible metal−oxygen battery chemistries, the Li/O_2 battery has the highest specific theoretical energy, 3.46 kW h kg^{-1}. The primary discharge product of a Li/O_2 cell is crystalline Li_2O_2; it has been shown that side reactions involving Li_2O_2, which can form stable phases such as Li_2CO_3, are an important contributor to high overpotentials.[13] It has also been proposed that high overpotentials persist even in the absence of side reactions because of the low intrinsic conductivity in Li_2O_2.[1,9]

In addition to Li_2O_2, superoxide species, O_2^-, such as in LiO_2, have also been occasionally reported during discharge of Li/O_2 cells by in situ spectroscopy.[14] Nevertheless, solid lithium superoxide, LiO_2, has proven difficult to synthesize in pure form, and only impure samples that decompose to Li_2O_2

Received: September 2, 2019
Revised: October 10, 2019
Published: October 11, 2019

DOI: 10.1021/acs.chemmater.9b03592
Chem. Mater. XXXX, XXX, XXX−XXX

Table 1. Reported Structural Properties of the Superoxides (Based on Refs[28,30−35])

	temperature [K]	structure (space group)	O_2 orientation	O_2 order
LiO_2	$T < 70$	marcasite ($pnnm$)	⟨111⟩	ordered
NaO_2	$223 < T$	NaCl-type/disordered pyrite ($Fm\bar{3}m$)	no order	hindered rotation
	$196 < T < 223$	pyrite ($Pa\bar{3}$)	⟨111⟩ on average	hindered rotation
	$T < 200$	marcasite ($pnnm$)	⟨111⟩	ordered
KO_2	$383 < T$	NaCl-type/disordered pyrite ($Fm\bar{3}m$)	no order	free rotation
	$196 < T < 383$	tetragonal ($I4/mmm$)	[001] on average	semi-free rotation
	$12 < T < 196$	monoclinic ($C2/c$)	inclined 19−22° to [001][a]	ordered
	$T < 12$	triclinic	inclined 30° to [001][a]	ordered

[a]Refers to the [001] direction of the corresponding tetragonal cell.

above 238 K have been achieved.[15] Therefore, in a typical Li/O_2 cell, one may anticipate that LiO_2 will disproportionate into Li_2O_2 and O_2.[16] Contrary to these expectations, Lu et al.[14] reported the surprising observation of crystalline LiO_2 formation during discharge of a Li/O_2 cell employing a graphene cathode decorated with iridium (Ir) nanoparticles. The LiO_2 formed was reported to be stable during multiple charge and discharge cycles and exhibited a relatively low overpotential. The low overpotential was attributed to several factors, one being the metallic behavior of LiO_2 predicted by density functional theory (DFT) band structure calculations with a generalized gradient approximation (GGA) functional and the hybrid Heyd−Scuseria−Ernzerhof (HSE) ($\alpha = 0.48$) functional.[14] However, subsequent calculations using hybrid functionals predicted insulating behavior for bulk LiO_2, with a band gap of 3.7−4.0 eV.[17,18]

Other metal−oxygen battery variants have been made by replacing lithium with different alkali metals. One example is the Na/O_2 system. The discharge mechanism in Na/O_2 batteries appears to be different from that of Li/O_2 batteries: some studies have reported Na_2O_2 as the main discharge product,[19] whereas others report NaO_2.[12] A Na/O_2 cell with Na_2O_2 as a discharge product exhibited a high charging overpotential of ∼1 V.[19] In contrast, significantly lower charging overpotentials (∼0.2 V) have been reported when the discharge product consists primarily of NaO_2.[12] A computational study clarified this by showing that Na_2O_2 is thermodynamically preferred above 120 K; however, its formation is limited by high kinetic barriers.[2] On the other hand, the formation of NaO_2 is associated with low kinetic barriers, making it the main discharge product under operating conditions.[2] Regarding electronic conductivity, both Na_2O_2 and NaO_2 behave similarly: hybrid functional calculations have shown that both materials are insulators with band gaps in excess of 5 eV.[10]

Potassium/O_2 batteries are yet another example of an emerging metal−oxygen system. In this chemistry, KO_2 appears to be the primary discharge product. KO_2 is thermodynamically stable, and it has been demonstrated that K/O_2 cells containing KPF_6 salt in DME form solely KO_2 (and not K_2O_2) during the oxygen reduction (discharge) reaction.[20] Importantly, the total overpotential for the first cycle of these cells was less than 50 mV.[6,20] Contradicting reports exist regarding the conductivity of KO_2. One early measurement reported high conductivity of approximately 1−10 S/cm.[21] More recently, Gerbig et al. examined the total (ionic + electronic) conductivity of KO_2 using the electromotive force method.[22] The value of the electronic conductivity could not be exactly determined in that investigation but was estimated to be less than 10^{-7} S/cm at 200 °C,[22] a much smaller value than in the initial report.[21]

Overall, the developing experimental consensus is that Li/O_2, Na/O_2, and K/O_2 batteries can exhibit relatively low overpotentials and enhanced rechargeability when the discharge product is an alkali superoxide.[2,16,20] Nevertheless, the charge-transfer mechanisms of alkali superoxides have not been systematically studied, and there exists a lack of consensus regarding the absolute value of the intrinsic conductivities of these compounds.

Motivated by this challenge, the present study presents a systematic computational investigation of the structure and charge-transport properties of alkali-metal superoxides based on Li, Na, and K. While an increasing number of computational studies of these phases have been reported,[2,10,14,17,18,23−27] drawing robust conclusions from these distinct efforts is not straightforward, as they often employ different computational methodologies, dissimilar equilibrium conditions, or different assumptions regarding crystal structures and/or types of charge-carrying species (typically point defects). In the case of KO_2, the problem of how to appropriately represent the room-temperature phase in ground-state DFT calculations remains unsettled because of dynamic oxygen dimer hindered rotation (see the following section for more details). In this study, first-principles calculations were used to search for an appropriate room-temperature structure for KO_2, accounting for the rotational degrees of freedom of superoxide dimers while keeping the symmetry of the cell compatible with the experimental structure. The optimal structure for KO_2 is identified. Following the same procedure, the orientation of superoxide ions within the LiO_2 marcasite and NaO_2 pyrite structures was verified. Estimates for the O_2 rotational barriers for each of the alkali superoxides are presented.

Based on the predicted structures, band gaps, defect formation energies/equilibrium concentrations, mobilities, and conductivities are comparatively analyzed across the alkali superoxides; comparisons with the related alkali peroxides are provided. We find that the alkali superoxides are band insulators with band gaps exceeding 4 eV. The negligible conductivity contributed by band-based mechanisms suggests that significant contributions from hopping of charged defects will be required to reach the levels of conductivity necessary for a practical a metal−oxygen battery cathode. By comparing with previous work on Li_2O_2, Na_2O_2, and NaO_2,[9,10] intrinsic conduction mechanisms across alkali-metal peroxides and superoxides are discussed.

Regarding ionic transport, vacancies situated on the cation sublattice dominate in the alkali peroxides, whereas O_2^- vacancies prevail in the alkali superoxides. These superoxide

DOI: 10.1021/acs.chemmater.9b03592
Chem. Mater. XXXX, XXX, XXX−XXX

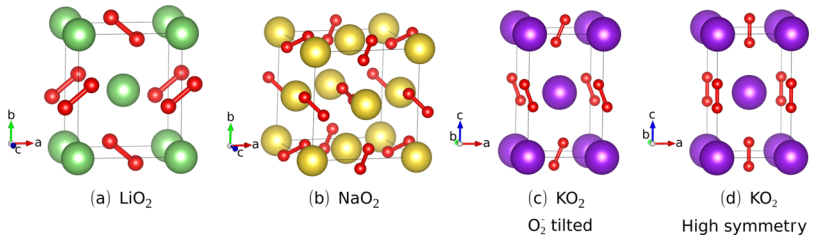

Figure 1. Crystal structures of (a) marcasite LiO_2, (b) pyrite NaO_2, (c) tetragonal KO_2, and (d) the average room-temperature structure of KO_2 in the tetragonal symmetry. Panels (a–c) depict the unit cells used that were periodically replicated in subsequent supercell calculations. Red spheres represent oxygen ions, green spheres represent Li ion, yellow spheres represent Na ion, and purple spheres are potassium ion.

vacancies are generally very mobile; consequently, the alkali superoxides exhibit several orders of magnitude larger ionic conductivities, 10^{-12} to 10^{-9} S/cm, than do the alkali peroxides, 10^{-20} to 10^{-19} S/cm.

For discharge product thicknesses where electron tunneling is negligible, electronic transport in the peroxides and superoxides is predicted to be mediated by the hopping of small polarons between neighboring oxygen dimers. For NaO_2 and KO_2, the electronic conductivity is predicted to be low and to range from 10^{-20} to 10^{-19} S/cm. These values are similar to that of the alkali peroxides[9,10] and thus suggest that the low overpotentials observed for Na- and KO_2-based batteries cannot be explained by enhanced electronic conductivities. Importantly, LiO_2 is predicted to have a much higher electronic conductivity compared to the Na and K analogues, 9×10^{-12} S/cm, arising from the migration of electron polarons. The much larger conductivity predicted for LiO_2 implies that the superior performance observed in LiO_2-based cells may reflect the ability of LiO_2 to support higher charge-transport rates.

CRYSTAL STRUCTURES OF THE ALKALI SUPEROXIDES

Table 1 summarizes the crystal structures adopted by the light alkali-metal superoxides as a function of temperature. At high temperature, the alkali superoxides adopt the rock salt structure, with the alkali ion at the cation site and the superoxide freely rotating at the anion site. Lowering the temperature increasingly reduces the superoxide rotational degrees of freedom, such that at very low temperatures the superoxide ions are essentially immobile. Concomitantly, the NaCl framework is increasingly distorted with decreasing temperature so as to accommodate the preferred (fixed) orientations of the superoxide ions.[28] In these superoxides, the alkali-metal ions donate an electron to the O_2 sublattice to form M^+ monovalent cations and O_2^- superoxide anions. Consequently, these compounds are highly ionic, with energy levels near the Fermi level dominated by states derived from the O-dimers. Thus, one can expect the electronic properties of the superoxide solids to resemble those of the superoxide molecule.

Another noteworthy property of the superoxide anion is its doubly degenerate $\pi^*_{x,y}$-orbitals, with one orbital being occupied and the other unoccupied. If the overlap of these $\pi^*_{x,y}$-orbitals between adjacent anions in the alkali-superoxide lattice was sufficiently large, the $\pi^*_{x,y}$-bands would be strongly dispersed. In this case, metallic behavior would emerge, with each of the two $\pi^*_{x,y}$-bands being half occupied. In contrast, poor overlap of the $\pi^*_{x,y}$-orbitals would result in molecular solid-type behavior, that is, independent superoxide anions in a "sea" of alkali cations. In this latter scenario, the Jahn–Teller theorem instructs that the local symmetry around a superoxide ion cannot be so high as to preserve the degeneracy of the $\pi^*_{x,y}$-orbitals. The Jahn–Teller effect (JTE) provides a driving force that reduces the symmetry, distorting the original geometry in such a way that the electronic degeneracy is lifted, opening a gap between the $\pi^*_{x,y}$-orbitals. A set of symmetry-equivalent Jahn–Teller distortions leads to different geometries around the superoxide ion, all of them being energy minima. If the energy barriers separating these energy minima are sufficiently high compared to the thermal energy, then the system will be kinetically trapped into one of the minima and will adopt a lower-symmetry structure (the so-called static JTE). This is the situation for all alkali superoxides at low temperatures. Alternatively, at higher temperatures, the local geometry can "hop" between the different structural minima, resulting in an average structure that is similar to the undistorted, high-symmetry configuration (the so-called dynamic JTE). This situation describes the behavior of KO_2 at room temperature. This behavior implies that care must be exercised when calculating electronic properties (such as the band gap) in this dynamic regime. Such a calculation should be performed using one of the lower-symmetry, Jahn–Teller-distorted geometries rather than the averaged, high-symmetry configuration. Adopting the latter, high-symmetry case results in an electronic configuration in which the $\pi^*_{x,y}$-degeneracy is not lifted and the appearance of a partially filled band in the density of states (DOS). Metallic behavior will result if sufficient overlap exists between these orbitals on adjacent anions.[29]

Many properties of the alkali superoxides are influenced by the local structure and orientation of the superoxide anion. The influence of the anion orientation has been studied in alkali halides wherein halide ions were substituted for superoxide ions.[30,31] Other studies have revealed how the structure and superoxide orientation evolve with temperature, Table 1.[28,32−34] Although in these studies averaged, high-symmetry room-temperature structures were determined, it remains a matter of debate as to how these room-temperature structures should be represented in DFT ground-state energy calculations, where the high symmetry must be broken for an appropriate electronic structure to be predicted. Furthermore, in LiO_2 and NaO_2, it is unclear if the measured structural properties are influenced by a dynamic JTE. No room-temperature X-ray diffraction (XRD) pattern has been established for LiO_2, and at least hindered rotation of superoxides is likely at room temperature in NaO_2.[32] For KO_2 it is known that the structure obtained from XRD measurements is an averaged structure originating from a dynamic local low-symmetry arrangement of atoms.[32,33,35] This

DOI: 10.1021/acs.chemmater.9b03592
Chem. Mater. XXXX, XXX, XXX−XXX

is similar to the dynamics of the organic cations observed in hybrid perovskites at room temperature.[36]

LiO_2 is observed to crystallize in the marcasite structure at liquid nitrogen temperature.[34] Although it seems reasonable that LiO_2 should transform to the pyrite structure at higher temperatures, similar to the behavior of other alkali superoxides, the lack of experimental structure data for LiO_2 at room temperature has lead previous studies to suggest the marcasite structure as the most representative.[16] Here, we follow this precedent and adopt the marcasite structure (space group *Pnnm*) for the present study. In this structure, the LiO_2 units exhibit an ABAB stacking sequence along the *c*-axis, and each layer has the same number of Li atoms and O_2 molecules, see Figure 1. The superoxide anions are located in the (001)-plane within one layer, with the angles between the superoxide and the *a*-axis equal to +41° and −41° for A and B layers, respectively.

At room temperature, KO_2 crystallizes in a body-centered-tetragonal structure (space group *I*4/*mmm*) of CaC_2 type, wherein the superoxides are on average orientated parallel to the tetragonal axis.[28] Because of the orbital degeneracy of the superoxide, the energy of the system can be lowered by a Jahn−Teller distortion. This can arise from both nutation of the superoxide molecular axis away from a high-symmetry direction[35] and from the displacement of the anion's center of mass from a high-symmetry position. In the low-temperature phases, the symmetry is lowered to a monoclinic symmetry (T < 196 K) or a triclinic symmetry (T < 12 K) where the superoxides are both displaced along the monoclinic b-axis and tilted with respect to the [001] direction of the tetragonal cell. All of these effects together can be seen as a static Jahn−Teller distortion of the tetragonal structure. Because such a JTE will persist at room temperature, the measured tetragonal structure (with the superoxides aligned with the [001] direction) is likely to be an averaged structure resulting from a dynamic JTE.[32,33,35] At room temperature, the actual arrangement of the atoms at the local level has not been unambiguously determined. However, a model assuming a dynamic JTE where the superoxides are nutated along the [100] direction and precess around the *c*-axis is in agreement with XRD data.[35] Electron paramagnetic resonance was used to quantify the nutation angle at 13 K to 22° and at 78 K to 19°; however, this is in the monoclinic phase where the directions of the superoxides are frozen in.[33]

A small number of theoretical reports examined the coupled structural and electronic properties in KO_2.[23,24,27] Nandy et al. optimized the KO_2 structure without symmetry constraints, resulting in a nontetragonal structure that was 22 meV/f.u. lower in energy than the high-symmetry structure.[27] Kim et al. enforced tetragonal symmetry but nutated all the superoxide anions by ∼30° in the same direction.[23,24] The resulting structure exhibited a band gap, indicating that KO_2 is an insulator.

Despite the existence of these prior studies, the precise orientation of the O_2 bond axis in KO_2 remains uncertain. Hence, it would be helpful to explore how a nonsymmetrized room-temperature structure for KO_2 could be represented. Similarly, it would be helpful to verify that the suggested LiO_2 and NaO_2 structures are in fact optimal with respect to their superoxide orientations. Finding a valid computational representation for these ambient temperature phases is important for achieving an accurate estimate of their band gaps. These gaps can vary from zero to several electron volts depending on the superoxide orientations in the crystals.[37] Of course, this detail has implications for the possibility of band-like conduction, but can also impact contributions to the conductivity from the hopping of charged defects, as the formation energies of these defects, and hence their concentrations, are calculated relative to the positions of the valence and conduction bands. Clarifying these issues requires a constrained minimization strategy that maintains the characteristics of the relevant room-temperature phases but avoids the (free) optimizations that can generate structures resembling the low-temperature phases, the latter being less representative of room-temperature battery discharge products. Furthermore, an estimate of the barrier for rotation of superoxide dimers would reveal if the structure and electronic properties of superoxides are affected by rotational degrees of freedom at room temperature, as well as give an estimate for the quality of the approximation associated with neglecting anion rotation when calculating free energies. The details of the constrained optimization approach is given is the next section.

METHODOLOGY

DFT calculations were performed using the Vienna Ab initio Simulation Package (VASP).[38−41] Ground-state geometries and electronic structures were determined using (separately) the GGA + U method [with the Perdew−Burke−Ernzerhof (PBE) functional[42] and the HSE hybrid functional.[43,44] A Γ-centered *k*-point grid with density 6 × 6 × 6 for LiO_2 and KO_2 was used for HSE calculations involving primitive cells. For PBE + U calculations, 8 × 8 × 8 and 8 × 8 × 4 Γ-centered *k*-point grids were used for LiO_2 and KO_2, respectively. The hybrid calculations employed a planewave energy cutoff of 460 eV and adopted the default VASP PAW potentials with valence electron configurations of 2s for Li, 2s2p for O, 2p3s for Na, and 3p4s for K. The PBE + U calculations used the hard PAW potentials with valence electron configurations of 1s2s for Li, 2s2p for O, 2s2p3s for Na, and 3s3p4s for K.[45] Consistent with the use of the harder PAW potentials for the PBE + U calculations, a larger planewave cutoff energy of 900 eV was adopted. For structure optimizations, all ions were relaxed to a force tolerance of less than 0.04 eV/Å for calculations involving KO_2, and to 0.02 eV/Å or less for LiO_2 and NaO_2. Non-self-consistent many-body perturbation theory (G_0W_0 method) was used for the calculation of band gaps, taking HSE wavefunctions as input. Convergence tests were performed with respect to the number of empty bands; based on these tests, a total of 512 bands were used.

Our calculations employ the PBE + U and HSE functionals as earlier studies have shown that semilocal functionals often poorly describe electronic properties of alkali superoxides.[10,46] Especially for defect calculations, semilocal functionals may fail to correctly describe localized charge distributions associated with charge-carrying defects such as polarons and can underestimate polaron hopping barriers.[9] These shortcomings of semilocal functionals can be at least partially rectified by introducing some fraction of exact exchange or a Hubbard ($+U$) correction. Based on previous calculations in which the impact of the fraction of exact exchange on band gap, formation energies, and migration barriers were examined in alkali super- and peroxides,[9,17] the present study adopts a fraction of 48% exact exchange (α = 0.48) for HSE calculations. This value allows consistent comparisons to be

DOI: 10.1021/acs.chemmater.9b03592
Chem. Mater. XXXX, XXX, XXX−XXX

made between the present calculations on superoxides and prior studies involving peroxides.

In the PBE + U calculations, the Hubbard correction was applied to the p-orbitals of the oxygen atoms; these are the chemically active orbitals on super- and peroxide anions. Prior studies have shown that a correction between 4 and 8 eV gives a reasonable description of the alkali super- and peroxides.[23,27,47,48] In principle, one should calculate the appropriate correction for every given compound and atomic configuration using, for example, a linear response method.[49] However, our interest here is less in determining the absolute value of band gaps and more on comparisons between systems having perturbations to their respective atomic structure. Therefore, we adopt a more pragmatic approach and, following Garcia-Lastra et al.,[48] set U = 6 eV for all PBE + U calculations.

Care should be taken when applying a +U correction to p-orbitals. In VASP the effect of the correction is dependent on the overlap of the atomic wavefunctions within the PAW augmentation sphere (the bounds for the integration can differ slightly form the augmentation sphere radius). Because p-orbitals are poorly contained within the augmentation sphere this can lead to unexpected and incomparable results between different code implementations when the +U correction is applied to p-orbitals. We reduce the effect of this issue by normalizing the overlap to one within the augmentation sphere. (Additional details are provided in the Supporting Information).

The present study aims to determine the room-temperature structure of KO_2 and to characterize the energy associated with precessions of its superoxide ions. Various nutation and precession orientations of the superoxides are examined, while maintaining the measured room-temperature tetragonal structure. The search is furthermore restricted to the two dimers of the conventional unit cell. These constraints limit the number of structures to be considered to a tractable amount and ensure that the resulting structure is a good starting point for computationally expensive defect calculations.

Figure 2 illustrates the adopted dimer precession model for KO_2. The conventional unit cell of KO_2 contains two O_2^-

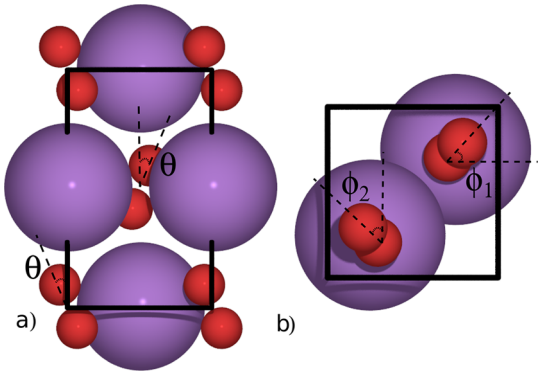

Figure 2. Precession model of KO_2 viewed along the (a) [010] and (b) [001] directions.

units; three angles were used to describe the orientation of these anions: θ, ϕ_1, and ϕ_2. First, we identify the optimal nutation angle, θ^{opt}. Next, fixing the nutation angle to θ^{opt}, the two dimers are allowed to precess independently. For every fixed set of angles (θ^{opt}, ϕ_1, ϕ_2), the structure is relaxed. The result is a potential energy surface which is used to identify the optimal dimer orientations. Given the computational expense of hybrid functionals, the search for the lowest energy angles was performed with the PBE + U method. Constrained relaxations were performed using the Atomic Simulation Environment.[50] The details of the procedure are as follows:

(1) Two sets of directions for the nutation angle of the dimers were explored; in both cases, the tetragonal symmetry of the cell is maintained during optimization. θ is searched in the interval [1°, 35°] with a resolution of 1 degree.
   (a) The dimers are nutated toward the sides of the cell, that is, one dimer is nutated along the [100] direction and the other along the [010] direction.
   (b) Or the dimers are nutated toward the corners of the cell, that is, one dimer is nutated along the [110] and the other along the [$\bar{1}$10] direction.
(2) For every fixed θ, the cell is relaxed followed by an optimization of the internal degrees of freedom. This results in optimal nutation angles of 21° and 23° for the nutation directions described in (a) and (b), respectively (Figure S1). We choose θ^{opt} to be the average of the two optimal nutation angles, that is, θ^{opt} = 22°.
(3) For every set of ϕ_1, ϕ_2, and θ^{opt}, the atoms are relaxed under the constraints that the angles and the lattice parameters are fixed. ϕ_1 and ϕ_2 are mapped out in the intervals [0°, 45°] and [0°, 355°], respectively, with a 5° resolution. The remainder of the potential energy surface dependent on ϕ_1 and ϕ_2 is equivalent by symmetry.

Similar structure analyses were performed for LiO_2 and NaO_2 (see the Supporting Information for additional details).

Defect calculations were performed on relaxed supercells of LiO_2 and KO_2. These cells were comprised of 3 × 3 × 2 expansions of the respective unit cells and contained a total of 108 atoms. K-point sampling was performed at the Γ-point for all defect calculations. Based on our prior calculations on NaO_2, five types of charged defects were considered:[10] negative vacancies on the metal (M) cation site (V_M^-), positive interstitials (M_i^+), superoxide vacancies ($V_{O_2}^+$), electron polarons (e_p^-), and hole polarons (h_p^+). As described above, the states around the Fermi level are dominated by $\pi^*_{x,y}$-orbitals. Thus, adding or removing an electron is associated with filling or emptying these antibonding orbitals. Consequently, both types of polarons are expected to localize on the superoxide dimer, with both causing distinct changes in the O−O bond length. The importance of these six defects in LiO_2 was also demonstrated by a recent study by Li et al.[17]

The chemical potential of oxygen was assumed to be fixed by equilibrium with oxygen in the atmosphere and given by the formula

$$\mu_O = \frac{1}{2}\mu_{O_2} = \frac{1}{2}[E_{O_2}^{DFT,corr} + k_B T - TS_{O_2}^{expt}]$$

where $E_{O_2}^{DFT,corr}$ is the corrected energy of O_2, the $k_B T$ term accounts for the pV contribution to the free energy, and $S_{O_2}^{expt}$ is the experimental entropy.[51] Contributions to the free energy from translational, rotational, and vibrational degrees of freedom have been neglected; these terms are also not included for the bulk phases. This is in line with a recent study which showed that contributions to the free energy from rotational and vibrational frequencies are to a good approximation negligible for the NaO_2 room-temperature

DOI: 10.1021/acs.chemmater.9b03592
Chem. Mater. XXXX, XXX, XXX−XXX

phase.[2] The chemical potentials of the alkali metals (Li, Na, K) within the superoxides were established by the relation

$$\mu_M + 2\mu_O = E_{tot}[MO_2]$$

where M = Li, Na, K is the alkali metal and $E_{tot}[MO_2]$ is the total energy per formula unit of the corresponding alkali superoxide. Knowing that DFT calculations tend to overbind gas-phase O_2, an O_2 correction of 0.10 eV was applied for the ground-state energy of the O_2 molecule. This correction value was determined using a linear fit between the calculated and experimental formation enthalpies for the alkali superoxides: marcasite LiO_2, pyrite NaO_2, and tetragonal KO_2. Coincidentally, we note that this value is equal to the value in our previous work on NaO_2,[10] where we calculated the correction using the experimental value of the NaO_2 formation enthalpy. This coincidence, however, allows us to directly compare the results of the present study on LiO_2 and KO_2 with our previous work on NaO_2.[10] Energy barriers associated with the migration of these charged defects were estimated using nudged-elastic-band calculations with seven images on the band.[52]

RESULTS AND DISCUSSION

Superoxide Structure Search. Figure 3 shows a potential energy map for the constrained structure search over superoxide anion orientations in KO_2. The optimal structure is obtained for $\theta = 22°$, $\phi_1 = 0° + 90° \times i$, and $\phi_2 = 90° + 90° \times i$ for $i \in [0, 1, 2, 3]$. This arrangements corresponds to one dimer nutated toward [100], [010], [$\bar{1}$00], or [0$\bar{1}$0] and the other dimer in the opposite direction. In this structure, the symmetry of the superoxides has indeed been broken, yet the external cell structure is consistent with experimental measurements for the room-temperature KO_2 phase. This structure was adopted in our subsequent bulk and defect calculations.

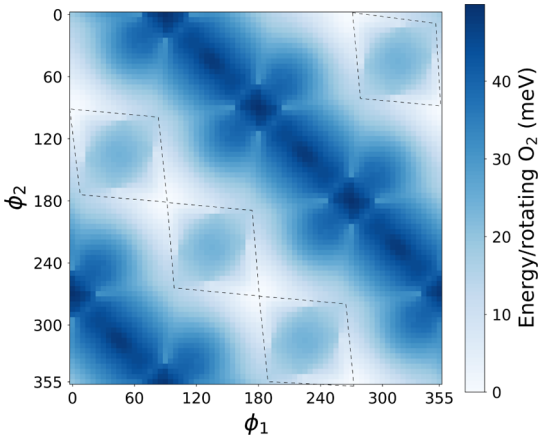

Figure 3. Potential energy map of O_2 orientations in KO_2 with a fixed $\theta = 22°$. The black dashed lines mark the minimum energy path for a full precession of the dimers.

The energy map in Figure 3 also reveals that the energy barrier associated with a full rotation of a superoxide is only 16 meV. Consequently, the energy of the RT phase relative to the ordered analogue can be approximated as half of the anion precession barrier, that is, the RT phase is higher in energy by ~8 meV/formula unit. That this barrier likely represents an upper bound to the real barrier; the computed barrier could be reduced further if the constrained degrees of freedom were relaxed. Since a temperature of 300 K corresponds to 26 meV, the thermal energy available at room temperature is sufficient to activate superoxide rotation around the z-axis. Such behavior is consistent with experimental measurements.[32,35] We further note that the potential energy surface is very flat. The least favored configuration of the superoxides is only 50 meV higher in energy than the most stable, corresponding to 8 meV/atom. This implies that the superoxide orientation has a small effect on the total energy of KO_2. The energy landscape reported in Figure 3 (calculated using PBE + U) was also verified at selected points using HSE calculations. Good agreement between the methods was obtained (Figure S2).

For LiO_2 and NaO_2, a similar search over O_2 orientations confirmed that the experimental structures (marcasite and pyrite, respectively) were the lowest in energy (see Figures S3−S6). Nevertheless, significant differences were predicted for the energy barriers for superoxide rotation across these three compositions, as shown in Table 2. In general, the precession barriers decrease for the heavier alkali superoxides. In LiO_2, a large barrier of 955 meV makes rotations of superoxides a rare event; thus, at ambient temperatures, these dimers are essentially locked at their equilibrium positions. In NaO_2, the precession barrier is significantly smaller, 53 meV. This prediction matches well with experiments, which show that NaO_2 transforms from the marcasite to the pyrite phase at 200 K, with the latter phase exhibiting evidence of hopping of dimers as the temperature increases towards room temperature.[32] The rotational barriers show that neglecting the O_2 rotational degrees of freedom in the free energy is well justified for NaO_2 and KO_2, as the rotations of the superoxides at room temperature will resemble that of free oxygen. However, for LiO_2 it may be a source of error.

Table 2. Energy Barriers for O_2 Precession Calculated from PBE + U

superoxide (structure)	precession barrier (meV)
LiO_2 (marcasite)	955
NaO_2 (pyrite)	53
KO_2 (tetragonal)	16

Table 3 summarizes the calculated structural and energetic properties (using HSE [α = 0.48]) of the superoxide phases examined here. In the case of LiO_2, the calculated lattice parameters are in good agreement with previous calculations using the HSE06 functional (a = 3.99 Å, b = 4.77 Å and c = 3.01 Å).[17] Ferromagnetic (FM) ordering was found to be 6 meV/f.u. more stable than anti-ferromagnetic (AFM) ordering. This is behavior is consistent with previous calculations that predicted FM ordering to be more favorable.[17] Regarding KO_2, the lattice parameters calculated from the precession model and the high-symmetry structure are both in reasonably good agreement with the experimental values of $a = b$ = 4.03 Å and c = 6.70 Å.[28] FM ordering was found to be 2 meV/f.u. more stable than AFM ordering in the precession model. This ordering is consistent with previous DFT calculations, which employed PBE + U with U values from 3 to 6 eV. In those calculations, the FM−AFM energy difference was in the range of −3 to −1 meV/f.u.[27]

Band Structure. Figures 4 and 5 show the calculated projected DOS at different levels of theory for LiO_2 and KO_2, respectively. From energies of −10 to 6 eV, the DOS is comprised primarily of oxygen-derived states, with little state density on the alkali-metal ions. These results, including our

DOI: 10.1021/acs.chemmater.9b03592
Chem. Mater. XXXX, XXX, XXX−XXX

Table 3. Calculated Low-Energy Magnetic Ordering, Energy Difference between Ferromagnetic and Antiferromagnetic Ordering, Lattice Parameters *a*, *b*, *c* (Å), O−O Intramolecular Bond Length *d*(O−O) (Å), and Distances between Metal Ions and Their Nearest O Atoms *d*(M−O_2) (Å)

structure	magnetization	$E_{FM} - E_{AFM}$ (meV/f.u.)	*a* (Å)	*b* (Å)	*c* (Å)	*d*(O−O) (Å)	*d*(M−O_2) (Å)
LiO_2 (marcasite)	FM	−6	4.011	4.783	3.042	1.30	2.52/2.39
NaO_2 (pyrite)	FM	−42	5.416	5.416	5.416	1.31	2.71
KO_2 (tetragonal, O_2^- tilted)	FM	−2	4.111	4.111	6.720	1.31	2.91/3.36
KO_2 (tetragonal, high symmetry)	FM	−36	3.991	3.991	6.843	1.31	2.91/3.36

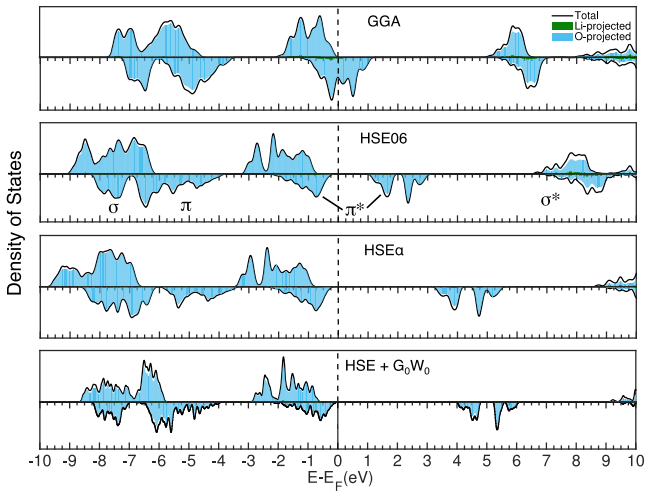

Figure 4. DOS (in arbitrary units) for LiO_2 calculated using four different levels of theory: (from top to bottom) PBE, HSE06, HSE (α = 0.48), HSE + G_0W_0. The energies are shifted such that the energy of the valence band maximum is assigned a value of zero.

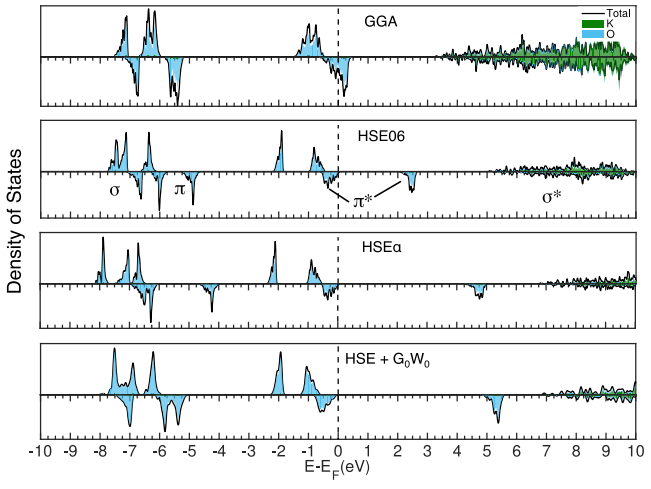

Figure 5. DOS (in arbitrary units) for the lowest energy (tilted) bulk KO_2 structure calculated using four different levels of theory: (from top to bottom) PBE, HSE06, HSE (α = 0.48), HSE + G_0W_0. The energies are shifted such that the energy of the valence band maximum is assigned a value of zero.

previous calculations on NaO_2,[10] imply that alkali superoxides are indeed highly ionic crystals. In the case of the semilocal PBE functional, LiO_2 and KO_2 are predicted to have half-metallic behavior, showing no band gap, which is in agreement with similar calculations in the literature.[14,46] In contrast, use of the HSE functional opens a band gap in both compounds by splitting the π^* states. Importantly, the symmetrized KO_2 structure (not shown) does not undergo this splitting and is predicted to be metallic, even with HSE because in this configuration the $\pi^*_{x,y}$-degeneracy is not lifted.

To more accurately estimate the band gaps of the superoxides, non-self-consistent G_0W_0 calculations were also performed (Figures 4 and 5). The HSE + G_0W_0 data indicate that LiO_2 has a band gap of 4.16 eV, close to the result of 4.02 eV by Li et al.[17] It also predicts that KO_2 has a band gap of 4.95 eV, suggesting that KO_2 is a wide band gap insulator.[24,27] Similarly, our earlier calculations on NaO_2 using the same functionals found a large band gap of 5.30 eV.[10]

Using PBE + *U*, the band gap of KO_2 is estimated to be 3.6 eV in the equilibrium configuration. An analysis of the band gap in KO_2 as a function of dimer orientation (using PBE + *U*) reveals that the size of the band gap varies from 2.6 to 3.7 eV depending on the orientation (see Figure S1). As previously discussed, the superoxide ions in KO_2 experience in a very flat potential energy surface. This suggests that the range of band gaps associated with these dimer configurations will be accessible at room temperature. Thus, although the G_0W_0 band gap (4.95 eV) is the most accurate estimate of the band gap at the equilibrium configuration, the actual band gap at room temperature will be influenced by the nearly-freely rotating superoxides. A similar but less drastic effect is expected in NaO_2, where the dimers are not as free to rotate, whereas in LiO_2 practically no contributions from rotating dimers is expected.

Despite these contributions from rotating superoxide anions, the predicted band gaps in the alkali-metal superoxides are so large that band-based conduction can be ruled out. Similarly, electron tunneling will only be able to sustain discharge currents for a very short period before a thick enough layer of deposited discharge product effectively blocks tunneling. Hence, the low overpotentials reported in alkali superoxide-based "air" batteries must arise from mechanisms other than band-based conduction and/or tunneling. One possibility is that the hopping of charged defects contributes to charge transport in these systems.

Intrinsic Defects—Formation Energies and Concentrations. The calculated formation energies of the five charged defects examined—hole and electron polarons, vacancies on the cation and anion sublattices, and cation interstitials—are summarized in Figure 6a for all three superoxide compositions. Detailed formation energy plots and calculated concentration data can be found in Figures S7 and S8 and Tables S1 and S2. The calculated formation energies were used to estimate the equilibrium concentrations at 300 K. These equilibrium concentrations may not be realized in an operating battery due to nonequilibrium effects (i.e., slow kinetics) arising, for example, from the rapid growth of a superoxide discharge product at ambient temperatures. Consequently, it is possible that the actual defect concentrations are higher than those predicted here.

DOI: 10.1021/acs.chemmater.9b03592
Chem. Mater. XXXX, XXX, XXX−XXX

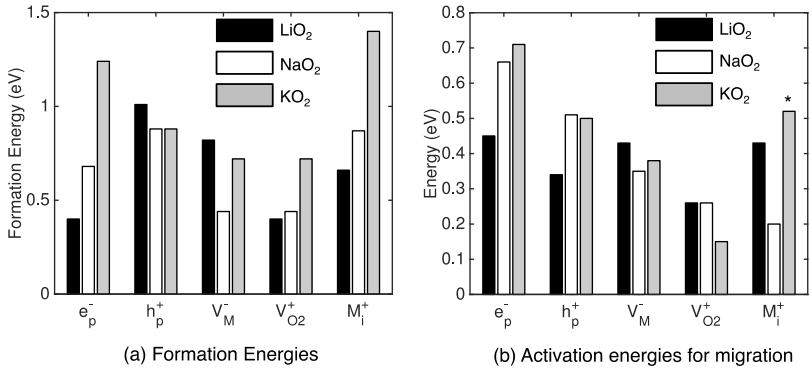

Figure 6. (a) Formation energies and (b) migration barriers for charged defects in LiO_2 (white), NaO_2 (black), and KO_2 (gray).

Turning first to defects in LiO_2, the dominant charged species are predicted to be superoxide vacancies, $V_{O_2}^{+}$ (comprising a missing superoxide anion), and electron polarons, e_p^-, localized on the superoxide anion. Both defects have a formation energy of 0.40 eV and a corresponding concentration of 7×10^{15} cm^{-3}. These findings differ from those recently reported by Li et al.,[17] whose calculations suggested that the dominant defects in LiO_2 are h_p^+ (hole polarons) and V_{Li}^- with concentrations of 1×10^{13} cm^{-3}. This difference can be explained by Li et al.'s. use of a different estimate for the oxygen chemical potential: in that study the total energy for oxygen at zero kelvin was adopted as the oxygen chemical potential, neglecting pV contributions and contributions from entropy (at experimental conditions).

In the case of KO_2, the dominant charged defects are both ionic species: the negatively charged potassium vacancy (V_K^-), and the superoxide vacancy ($V_{O_2}^{+}$), both having formation energies of 0.72 eV and equilibrium concentrations of 2×10^{10} cm^{-3}. Vacancy-based carriers were also reported to be dominant in NaO_2.[10] Drawing on the results of our earlier study on NaO_2,[10] we observe that a common feature across the three alkali superoxides is the existence of the superoxide vacancy as the dominant (highest concentration) positively charged defect. Based on the formation energies in Figure 6a, the equilibrium concentrations of $V_{O_2}^{+}$ are similar in LiO_2 and NaO_2 and approximately 5−6 orders magnitude smaller in KO_2. Compared to the alkali peroxides, the concentrations of the dominant ionic defects in the alkali superoxides are about 8 orders of magnitude larger.[9,10] Our prediction that $V_{O_2}^{+}$ constitutes the dominant charge-carrying defect is in good agreement with Gerbig et al.'s experimental measurements, where superoxide vacancies were also reported to be the main contributor to the total conductivity in the heavy alkali superoxides (KO_2, RbO_2, and CsO_2).

Turning now to polaron phenomena, as previously described, a hole (electron) polaron consists of a missing (additional) electron localized on a superoxide anion, resulting in a distortion of the local lattice structure: the O−O bond length and distance between the superoxide hosting the polaron and nearest-neighbor alkali-metal atoms, which form an octahedron around the superoxide, are altered. For a hole (electron) polaron, the O−O bond length contracts (expands) and the neighboring M^+ ions are repelled (attracted) by the missing (added) electron. A hole polaron changes the host superoxide (O_2^-) to a neutral state (O_2^0), similar to that of gaseous oxygen, with two unpaired electrons in the $\pi^*_{x,y}$ orbitals and a magnetic moment of $2\mu_B$. An electron polaron changes its host superoxide to a peroxide ion (O_2^{2-}) which has fully occupied $\pi^*_{x,y}$ orbitals and a magnetic moment of zero. This behavior is common across the alkali superoxides as is confirmed by the present results, work by Li et al.,[17] and in our previous calculations on NaO_2.[10] The structural and magnetic changes introduced by the polarons are shown in Figures 7 and 8 for LiO_2 and KO_2, respectively. (In LiO_2 and KO_2, each octahedron has two distinct M−O_2 bond distances; these are noted as in-plane/out-of-plane in Table 3).

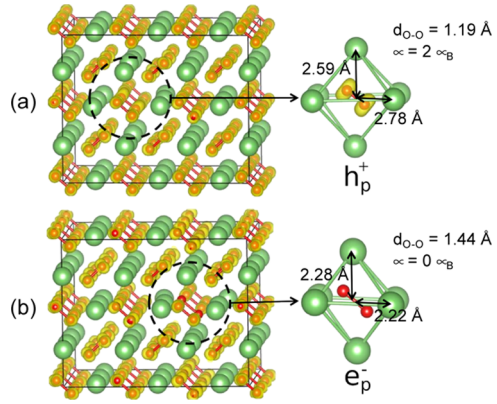

Figure 7. Magnetization density distribution for (a) hole and (b) electron polarons in LiO_2. Structural and magnetic properties of the respective O−O dimers and nearest-neighbor Li-ions are shown to the right. Isosurfaces depict the spin density at a value of 0.04 e $Bohr^{-3}$.

For LiO_2, the calculated formation energies of the electron and hole polarons are 0.40 and 0.95 eV, respectively. In KO_2, the formation energy of the hole polaron, 0.88 eV, is similar to that of LiO_2, while forming an electron polaron requires significantly more energy, 1.24 eV. In KO_2, the oxygen dimer hosting the electron polaron reorients to be parallel with the z-axis, leaving it in a high-symmetry configuration. This is the only polaron which is found to be associated with a reorientation of the oxygen dimer; as a result of this significant structural change, the electron polaron in KO_2 is the polaron with the largest formation energy.

Compared to the peroxides, the energy of forming an electron polaron in Li and Na superoxide (0.40 and 0.68 eV, respectively) is much lower: the relevant formation energies are 1.51 eV[9] in Li_2O_2 and 2.07 eV[10] in Na_2O_2. This is explained by the fact that in a superoxide an electron polaron occupies a $\pi^*_{x,y}$-orbital, whereas in a peroxide it must occupy a higher energy σ^*-orbital. Differently, formation of a hole

DOI: 10.1021/acs.chemmater.9b03592
Chem. Mater. XXXX, XXX, XXX−XXX

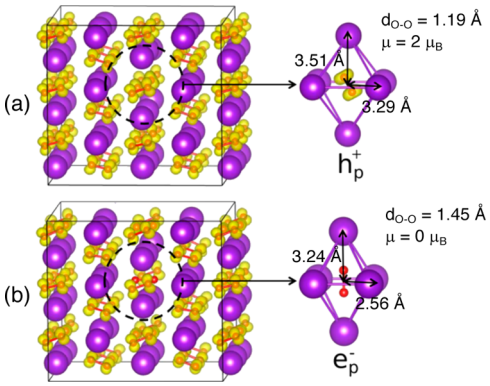

Figure 8. Magnetization density distribution for (a) hole and (b) electron polarons in KO_2. Structural and magnetic properties of the respective O−O dimers and nearest-neighbor K-ions are shown to the right. Isosurfaces depict the spin density at a value of 0.04 e $Bohr^{-3}$.

polaron involves removing an electron from the $\pi^*_{x,y}$ orbital in both superoxides and peroxides. Thus, the formation energies are very similar, that is, 0.95 and 0.88 eV for the superoxides and 0.95 eV[9] and 0.90 eV[10] for the peroxides.

The situation regarding concentrations of electronic carriers (polarons) in the alkali superoxides versus alkali peroxides is mixed. LiO_2 exhibits an 8 orders of magnitude larger concentration of polarons than does Li_2O_2,[9] while in NaO_2 these concentrations are 4 orders of magnitudes greater than that in Na_2O_2.[10] Electronic carrier concentrations in KO_2 resemble those in lithium and sodium peroxides.

Intrinsic Defects—Mobility. The preceding discussion reveals that the alkali superoxides generally exhibit relatively high concentrations of ionic defects in comparison to the analogous peroxides. Moreover, LiO_2 also supports a moderate equilibrium concentration of electronic carriers (e_p^-). However, for these defects to significantly contribute to intrinsic conductivities—and thus low overpotentials—they must also possess sufficient mobility. Mobility of the charge-carrying species is determined by the migration barriers that characterize elementary jumps between equilibrium sites.

A summary of calculated migration barriers for all three superoxide compositions is shown in Figure 6b. Figures S9 and S10 illustrate the migration pathways calculated using the nudged elastic band method. We first consider the mobilities of ionic species in LiO_2. For each species, there are three symmetry distinct migration pathways. Li et al. reported that the migration barriers for these pathways correlate with the hop length; therefore, we limit our calculations to the shortest hopping pathway, that is, migration along the z-axis. Our calculations suggest that all of the defects considered have small-to-moderate migration barriers, with $V_{O_2}^+$ having the smallest barrier of only 0.26 eV, corresponding to a diffusion coefficient of 4×10^{-7} cm^2 s^{-1}. [The diffusion coefficient, D, was evaluated as in our prior study:[10] $D = \nu a^2 e^{-E_b/k_BT}$, where ν is the hopping attempt frequency, which we take to be equal to the value typically used in semiconductors, 10^{13} s^{-1}. The jump distance is given by a, and E_b is the diffusion barrier (neglecting entropy contributions).] Although the orientations of the migrating superoxide dimer before and after the vacancy hop are parallel, the dimer is observed to rotate 90° during the migration process, leading to a V-shaped energy profile, similar to that in NaO_2.[10] The O−O bond does not break during the migration. Migration of the negative lithium vacancy, the second most prevalent charged defect, occurs via a pathway where the vacancy hops from one vertex of a distorted Li-ion octahedron to a nearest-neighbor vertex. The calculated energy barrier for this process, 0.43 eV, is comparable to the lowest barrier for vacancy migration in Li_2O_2,[9] 0.33 eV.

Regarding the mobilities of electronic carriers in LiO_2, the calculated barriers for migration of electron and hole polarons are 0.45 and 0.34 eV, respectively. These values are smaller than those reported for the same species in Li_2O_2: 1.41 and 0.42 eV for electron and hole polarons, respectively.[48,53] This suggests that LiO_2 will permit faster migration of both polaron types, possibly resulting in greater electronic conductivity.

In KO_2, for the case of ionic species, we focus on the two dominant carriers, negative potassium vacancies, V_K^-, and positive oxygen vacancies, $V_{O_2}^+$. (The barrier for migration of potassium interstitials was difficult to converge, and is not discussed further due to the very high formation energy, 1.40 eV, of this defect.) For each species, there are two symmetry distinct migration pathways: intralayer (along [100] or [010]) and interlayer (along [111]). For negative potassium vacancies, intralayer migration along the short path is favored. Migration occurs via a single hop from one vertex of a K-ion octahedron to a nearest-neighbor vertex with a barrier of 0.38 eV. For the superoxide vacancy, the interlayer migration is more favored than intralayer migration. The superoxides in the same layer are parallel, while in the interlayer path, they have orientations that differ by 44°. The intralayer migration is achieved by the simple translation of a superoxide in the opposite direction of the vacancy. In contrast, interlayer vacancy migration is accompanied by the rotation and translation of a superoxide, leading to a V-shaped migration pathway, similar to what is observed in LiO_2 and NaO_2.[10] No significant change to the O−O bond is observed during this migration. By far, the most mobile defect is the superoxide vacancy, with a migration barrier of only 0.15 eV, corresponding to a diffusion coefficient of 5×10^{-5} cm^2 s^{-1}. In general, superoxide vacancies are predicted to be very mobile in the alkali-metal superoxides, with barriers falling within 0.15−0.26 eV. This agrees well with Gerbig et al.'s experimental measurements, which reported high mobilities of O_2 in KO_2.[22]

The lattice constant of the alkali-metal superoxides also influences the size of the polaron migration barriers by altering the hopping distance (Li et al. also reported a correlation between hop length and barrier height in LiO_2).[17] In LiO_2, NaO_2, and KO_2 the polaron hopping distances are 3.03, 3.83, and 4.11 Å, respectively, with corresponding electron migration barriers 0.45, 0.66, and 0.71 eV and hole migration barriers 0.34, 0.51, and 0.50 eV.[10]

Conductivity. The calculated intrinsic conductivities (based on the respective equilibrium carrier concentrations) for LiO_2 and KO_2 are summarized in Table 4 and Figure 9 and compared with our prior calculations on Li_2O_2, NaO_2, and Na_2O_2.[9,10] Turning first to LiO_2, our calculations predict ionic and electronic conductivities of 4×10^{-9} and 9×10^{-12} S/cm, respectively. These values are 10 (4×10^{-19} S/cm) and 8 orders of magnitude larger (5×10^{-20} S/cm) than in Li_2O_2. Furthermore, LiO_2 has the highest electronic conductivity across all of the light alkali-metal peroxides and superoxides; calculated conductivities in these other phases are 7 to 8 orders of magnitude smaller. The ionic conductivity in LiO_2 is mainly mediated by superoxide vacancies which are the charged defect with both highest concentration and mobility. The ionic

DOI: 10.1021/acs.chemmater.9b03592
Chem. Mater. XXXX, XXX, XXX−XXX

Table 4. Calculated Ionic and Electronic Conductivities (S cm^{-1}) for LiO_2 and KO_2, and Comparison with Prior Calculations on Li_2O_2, Na_2O_2, and NaO_2.[a]

compound	ionic conductivity (S/cm)	electronic conductivity (S/cm)	highest concentration carriers
LiO_2	4×10^{-9}	9×10^{-12}	$V_{O_2}^{+}$, e_p^{-}
Li_2O_2	9×10^{-19}	5×10^{-20}	V_{Li}^{-}, h_p^{+}
NaO_2	4×10^{-9}	1×10^{-19}	$V_{O_2}^{+}$, V_{Na}^{-}, e_p^{-}, h_p^{+}
Na_2O_2	5×10^{-20}	1×10^{-20}	V_{Na}^{-}, h_p^{+}
KO_2	5×10^{-12}	1×10^{-20}	$V_{O_2}^{+}$, h_p^{+}

[a]Data for Li_2O_2, NaO_2, and Na_2O_2 are from refs 9 and 10.

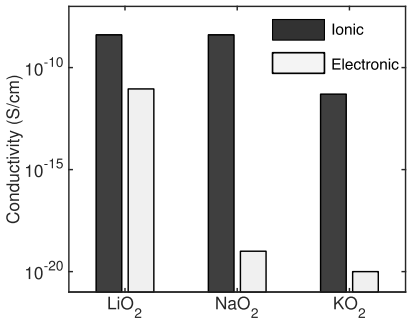

Figure 9. Ionic (black bars) and electronic (gray bars) conductivities (log scale) for LiO_2, NaO_2, and KO_2.

conductivity in NaO_2 is predicted to be similar to that of LiO_2 and primarily arises from contributions from $V_{O_2}^{+}$.[10]

In KO_2, the calculated ionic conductivity of 5×10^{-12} S/cm is 3 orders smaller than in LiO_2 and NaO_2, but 8 orders larger than in Li_2O_2 and Na_2O_2. These predictions are consistent with the experiments and conclusions reached by Gerbig et al.,[22] who measured the ionic conductivities of the heavier alkali-metal superoxides (KO_2, RbO_2, and CsO_2.) at 200 °C, and extrapolated a room-temperature ionic conductivity of $\sim 10^{-13}$ S/cm. Their ^{18}O isotope exchange experiments showed that the oxygen transport through KO_2 was based on the migration of intact oxygen dimers and this migration contributes to the ionic conductivity. (An "intact oxygen dimer" refers to a superoxide anion that migrates as a single unit without breaking its O−O bond). The predicted electronic conductivity is of KO_2 is 10^{-20} S/cm, similar to that of Li_2O_2,[9] suggesting that electronic transport through pristine KO_2 will be negligible, unless pathways coupled to microstructural features (surfaces, grain boundaries, amorphous regions, etc.) or nonequilibrium carrier concentrations contribute significantly. Our results are consistent with the conclusions reached by Gerbig et al., who found that the electronic conductivities of KO_2 were comparable to those of Li_2O_2.[54]

According to our previous work,[9] to limit the iR drop across the discharge product of a metal/O_2 battery to less than 0.1 V, the conductivity of that phase must be at least 2×10^{-11} S/cm. The calculated electronic conductivity of LiO_2 (9×10^{-12} S/cm) reported here, while slightly below this target, results in a moderate overpotential of ~0.15 V. This suggests that the higher electronic conductivity of LiO_2 is consistent with the observation of low overpotentials in this system. This conclusion does not hold, however, for NaO_2 or KO_2.

The main charge carriers in the peroxides, Li_2O_2 and Na_2O_2, were reported to be negative alkali-metal vacancies and (positive) hole polarons.[9,10] This differs from the superoxides, where polarons and (positive) superoxide vacancies dominate. All of the superoxides are predicted to have much larger ionic conductivities than do the peroxides. This behavior primarily originates from the high concentrations and mobilities of $V_{O_2}^{+}$. The low electronic conductivities predicted for KO_2 and NaO_2 suggest that the low overpotentials observed in batteries with these compounds as the main discharge product cannot be explained by larger electronic conductivities in these phases. However, it is important to recognize that the operating conditions present in a realistic cell could generate (nonequilibrium) defect concentrations that are much larger than the equilibrium values predicted in the present study. Such an effect could result in much higher electronic conductivities and potentially lower charging overpotentials. Therefore, an important area for future study is quantifying the identity and (nonequilibrium) concentrations of charge-carrying defects in peroxides and superoxides formed during the relatively rapid electrodeposition conditions present in a room-temperature metal/oxygen cathode.

The electron polaron is the dominant electronic carrier in LiO_2 and NaO_2, while the hole polaron prevails in KO_2. The latter is in apparent contradiction to the report of Gerbig et al. whose defect model predicts electron polarons to be the dominant electronic defect in KO_2.[22] Our results are in fact in qualitative agreement with this behavior. The pO_2 assumed here corresponds to the high limit of the partial pressures investigated by Gerbig et al. and a decreasing pO_2 will shift the formation energy of the ionic defects such that at some point the electron polaron and the superoxide vacancy will be the dominant defects.

■ CONCLUSIONS

Charge-transport mechanisms within the discharge products of alkali-metal/O_2 batteries can strongly influence the performance of these systems. To date, discharge products comprising alkali peroxides and superoxides have been observed. In general, cells that discharge to a superoxide exhibit lower overpotentials than those that form the corresponding peroxide. These lower overpotentials have been hypothesized to originate from more efficient charge transport within the superoxides. The present study critically assesses this hypothesis by systematically calculating the intrinsic conductivity and charge-transport mechanisms within the light alkali-metal (Li, Na, K) superoxides using DFT and quasiparticle methods.

While the transport mechanisms in the peroxides have been well studied, consensus regarding the conductivity within the superoxides is lacking. Our study draws on our prior investigations of the alkali peroxides and of sodium superoxide, while adding new analyses for LiO_2 and KO_2. In the case of KO_2 a nonsymmetrized room-temperature structure was proposed to account for a dynamic JTE. Band gaps, equilibrium (charged) defect concentrations, mobilities, and conductivities were estimated for both LiO_2 and KO_2.

Overall, the alkali superoxides are predicted to be wide band gap insulators, with gaps exceeding 4 eV. These large band gaps, combined with limited evidence for the Fermi level being located close to either band edge, implies that negligible transport occurs via band conduction. Thus, whatever charge

DOI: 10.1021/acs.chemmater.9b03592
Chem. Mater. XXXX, XXX, XXX−XXX

transport is present in these materials must occur via ion migration and/or electron/hole hopping.

Compared to the alkali peroxides, ionic conductivities in the superoxides are predicted to be 8−11 orders of magnitude larger, ranging from 4×10^{-9} to 5×10^{-12} S/cm at room temperature. A distinguishing feature of the superoxides is that their ionic conductivity is mediated primarily by superoxide vacancies. In the case of KO_2, the mobility of oxygen dimers is consistent with a recent experimental study by Gerbig et al., who found that superoxide ions are highly mobile in KO_2, RbO_2, and CsO_2.

Regarding electronic conductivities, transport in NaO_2 and KO_2 is predicted to occur via polaron hopping, with low conductivities on the order of 10^{-19} to 10^{-20} S/cm. These values are similar to what has been previously reported for the peroxides. Importantly, the present calculations indicate that LiO_2 has a much larger electronic conductivity (also arising from polaron hopping) than its Na and K analogues, 9×10^{-12} S/cm at 300 K. These data suggest that the low overpotentials observed for Na- and KO_2-based batteries cannot be explained by high intrinsic electronic conductivities. In contrast, the much larger conductivities predicted for LiO_2 imply that the superior performance observed in LiO_2-based cells may reflect the ability of LiO_2 to support higher charge-transport rates.

■ ASSOCIATED CONTENT

Supporting Information

The Supporting Information is available free of charge on the ACS Publications website at DOI: 10.1021/acs.chemmater.9b03592.

> Application of the +*U* approach to p-orbitals; dependence of the band gap in KO_2 on the tilt angle of superoxide dimers; calculated orientation of superoxide dimers in LiO_2 and NaO_2; comparison of GGA + *U* and HSE predictions for the energy of superoxide dimer orientations in KO_2; and calculated formation energies, concentrations, and migration barriers for point defects in LiO_2 and KO_2 (PDF)

■ AUTHOR INFORMATION

Corresponding Authors

*E-mail: jmgla@dtu.dk. Phone: +45 45 25 82 13 (J.M.G.-L.).
*E-mail: djsiege@umich.edu. Phone: +1 (734) 764-4808 (D.J.S.).

ORCID

Nicolai Rask Mathiesen: 0000-0001-7699-7976
Juan Maria García-Lastra: 0000-0001-5311-3656
Tejs Vegge: 0000-0002-1484-0284
Donald J. Siegel: 0000-0001-7913-2513

Author Contributions

¶N.R.M. and S.Y. contributed equally.

Notes

The authors declare no competing financial interest.

■ ACKNOWLEDGMENTS

N.R.M. and J.M.G.-L. acknowledge the support from the Villum Foundation's Young Investigator Programme (4th round, project: in silico design of efficient materials for next generation batteries. Grant number: 10096). D.J.S. acknowledges the support from the U.S. National Science Foundation, grant CBET-1351482. The support for the visit of D.J.S. to DTU was provided in part by DTU Energy, the Villum Foundation's Visiting Professor Program, and the Nordea Foundation's Residence Program.

■ REFERENCES

(1) Vegge, T.; Garcia-Lastra, J. M.; Siegel, D. J. Lithium−Oxygen Batteries: At a Crossroads? *Curr. Opin. Electrochem.* **2017**, *6*, 100−107.

(2) Mekonnen, Y. S.; Christensen, R.; Garcia-Lastra, J. M.; Vegge, T. Thermodynamic and Kinetic Limitations for Peroxide and Superoxide Formation in Na-O_2 Batteries. *J. Phys. Chem. Lett.* **2018**, *9*, 4413−4419.

(3) Lysgaard, S.; Christensen, M. K.; Hansen, H. A.; García-Lastra, J. M.; Norby, P.; Vegge, T. Combined DFT and Differential Electrochemical Mass Spectrometry Investigation of the Effect of Dopants in Secondary Zinc−Air Batteries. *ChemSusChem* **2018**, *11*, 1933−1941.

(4) *The Lithium Air Battery*; Imanishi, N., Luntz, A. C., Bruce, P., Eds.; Springer New York: New York, NY, 2014.

(5) Jung, K.-N.; Kim, J.; Yamauchi, Y.; Park, M.-S.; Lee, J.-W.; Kim, J. H. Rechargeable Lithium−Air Batteries: A Perspective on the Development of Oxygen Electrodes. *J. Mater. Chem. A* **2016**, *4*, 14050−14068.

(6) Xiao, N.; Ren, X.; McCulloch, W. D.; Gourdin, G.; Wu, Y. Potassium Superoxide: A Unique Alternative for Metal-Air Batteries. *Acc. Chem. Res.* **2018**, *51*, 2335.

(7) Yadegari, H.; Sun, X. Recent Advances on Sodium−Oxygen Batteries: A Chemical Perspective. *Acc. Chem. Res.* **2018**, *51*, 1532−1540.

(8) Christensen, J.; Albertus, P.; Sanchez-Carrera, R. S.; Lohmann, T.; Kozinsky, B.; Liedtke, R.; Ahmed, J.; Kojic, A. A Critical Review of Li/Air Batteries. *J. Electrochem. Soc.* **2011**, *159*, R1−R30.

(9) Radin, M. D.; Siegel, D. J. Charge Transport in Lithium Peroxide: Relevance for Rechargeable Metal−Air Batteries. *Energy Environ. Sci.* **2013**, *6*, 2370.

(10) Yang, S.; Siegel, D. J. Intrinsic Conductivity in Sodium−Air Battery Discharge Phases: Sodium Superoxide vs Sodium Peroxide. *Chem. Mater.* **2015**, *27*, 3852−3860.

(11) Mekonnen, Y. S.; Knudsen, K. B.; Mýrdal, J. S. G.; Younesi, R.; Højberg, J.; Hjelm, J.; Norby, P.; Vegge, T. Communication: The Influence of CO_2 Poisoning on Overvoltages and Discharge Capacity in Non-Aqueous Li-Air Batteries. *J. Chem. Phys.* **2014**, *140*, 121101.

(12) Hartmann, P.; Bender, C. L.; Vračar, M.; Dürr, A. K.; Garsuch, A.; Janek, J.; Adelhelm, P. A Rechargeable Room-Temperature Sodium Superoxide (NaO_2) Battery. *Nat. Mater.* **2013**, *12*, 228−232.

(13) Højberg, J.; McCloskey, B. D.; Hjelm, J.; Vegge, T.; Johansen, K.; Norby, P.; Luntz, A. C. An Electrochemical Impedance Spectroscopy Investigation of the Overpotentials in Li-O_2 Batteries. *ACS Appl. Mater. Interfaces* **2015**, *7*, 4039−4047.

(14) Lu, J.; Jung Lee, Y.; Luo, X.; Chun Lau, K.; Asadi, M.; Wang, H.-H.; Brombosz, S.; Wen, J.; Zhai, D.; Chen, Z.; et al. A Lithium−Oxygen Battery Based on Lithium Superoxide. *Nature* **2016**, *529*, 377−382.

(15) Hesse, W.; Jansen, M.; Schnick, W. Recent Results in Solid State Chemistry of Ionic Ozonides, Hyperoxides, and Peroxides. *Prog. Solid State Chem.* **1989**, *19*, 47−110.

(16) Yang, J.; Zhai, D.; Wang, H.-H.; Lau, K. C.; Schlueter, J. A.; Du, P.; Myers, D. J.; Sun, Y.-K.; Curtiss, L. A.; Amine, K. Evidence for Lithium Superoxide-like Species in the Discharge Product of a Li−O_2 Battery. *Phys. Chem. Chem. Phys.* **2013**, *15*, 3764.

(17) Li, S.; Liu, J.; Liu, B. First-Principles Study of the Charge Transport Mechanisms in Lithium Superoxide. *Chem. Mater.* **2017**, *29*, 2202.

(18) Lee, B.; Kim, J.; Yoon, G.; Lim, H.-D.; Choi, I.-S.; Kang, K. Theoretical Evidence for Low Charging Overpotentials of Superoxide Discharge Products in Metal-Oxygen Batteries. *Chem. Mater.* **2015**, *27*, 8406−8413.

DOI: 10.1021/acs.chemmater.9b03592
Chem. Mater. XXXX, XXX, XXX−XXX

(19) Sun, Q.; Yang, Y.; Fu, Z.-W. Electrochemical Properties of Room Temperature Sodium−Air Batteries with Non-Aqueous Electrolyte. *Electrochem. Commun.* **2012**, *16*, 22−25.
(20) Ren, X.; Wu, Y. A Low-Overpotential Potassium-Oxygen Battery Based on Potassium Superoxide. *J. Am. Chem. Soc.* **2013**, *135*, 2923−2926.
(21) Khan, A. U.; Mahanti, S. D. Collective Electron Effects of O_2− in Potassium Superoxide. *J. Chem. Phys.* **1975**, *63*, 2271.
(22) Gerbig, O.; Merkle, R.; Maier, J. Electrical Transport and Oxygen Exchange in the Superoxides of Potassium, Rubidium, and Cesium. *Adv. Funct. Mater.* **2015**, *25*, 2552−2563.
(23) Kim, M.; Min, B. I. Temperature-Dependent Orbital Physics in a Spin-Orbital-Lattice-Coupled 2p-Electron Mott System: The Case of KO_2. *Phys. Rev. B: Condens. Matter Mater. Phys.* **2014**, *89*, 121106.
(24) Kim, M.; Kim, B. H.; Choi, H. C.; Min, B. I. Antiferromagnetic and Structural Transitions in the Superoxide KO_2 from First Principles: A 2p-Electron System with Spin-Orbital-Lattice Coupling. *Phys. Rev. B: Condens. Matter Mater. Phys.* **2010**, *81*, 100409.
(25) Arcelus, O.; Li, C.; Rojo, T.; Carrasco, J. Electronic Structure of Sodium Superoxide Bulk, (100) Surface, and Clusters Using Hybrid Density Functional: Relevance for Na-O_2 Batteries. *J. Phys. Chem. Lett.* **2015**, *6*, 2027.
(26) Lau, K. C.; Curtiss, L. A.; Greeley, J. Density Functional Investigation of the Thermodynamic Stability of Lithium Oxide Bulk Crystalline Structures as a Function of Oxygen Pressure. *J. Phys. Chem. C* **2011**, *115*, 23625−23633.
(27) Nandy, A. K.; Mahadevan, P.; Sen, P.; Sarma, D. D. KO_2: Realization of Orbital Ordering in a p -Orbital System. *Phys. Rev. Lett.* **2010**, *105*, 056403.
(28) Ziegler, M.; Rosenfeld, M.; Känzig, W.; Fischer, P. Strukturuntersuchungen an Alkalihyperoxiden Alkalihyperoxiden. *Helv. Phys. Acta* **1976**, *49*, 57−90.
(29) Jahn, H. A.; Teller, E. Stability of Polyatomic Molecules in Degenerate Electronic States. I. Orbital Degeneracy. *Proc. R. Soc. A* **1937**, *161*, 220−235.
(30) Känzig, W. Paraelasticity, a Mechanical Analog of Paramagnetism. *J. Phys. Chem. Solids* **1962**, *23*, 479−499.
(31) Zeller, H. R.; Känzig, W. Die Elektronische Struktur Des O_2 Zentrums in Den Alkalihalogeniden . I ., Die Paramagnetischen Und Optischen Spektren Und Ihre Interpretation. *Helv. Phys. Acta* **1967**, *40*, 845−872.
(32) Känzig, W.; Labhart, M. Molecular and Magnetic Order in Alkali Hyperoxides A Short Review of Recent Work. *J. Phys., Colloq.* **1976**, *37*, C7-39−C7-45.
(33) Labhart, M.; Raoux, D.; Känzig, W.; Bösch, M. A. Magnetic Order in 2p-Electron Systems: Electron Paramagnetic Resonance and Antiferromagnetic Resonance in the Alkali Hyperoxides KO_2, RbO_2, and CsO_2. *Phys. Rev. B* **1979**, *20*, 53−70.
(34) Bakulina, V. M.; Tokareva, S. A.; Vol'nov, I. I. X-Ray Analysis of Lithium Superperoxide LiO_2. *J. Struct. Chem.* **1967**, *8*, 980−981.
(35) Halverson, F. Comments on Potassium Superoxide Structure. *J. Phys. Chem. Solids* **1962**, *23*, 207−214.
(36) Bechtel, J. S.; Seshadri, R.; Van der Ven, A. Energy Landscape of Molecular Motion in Cubic Methylammonium Lead Iodide from First-Principles. *J. Phys. Chem. C* **2016**, *120*, 12403−12410.
(37) Kemeny, G.; Kaplan, T. A.; Mahanti, S. D.; Sahu, D. Charge-Density Waves and the Displacive Collective Jahn-Teller Effect in Alkali Superoxides. *Phys. Rev. B* **1981**, *24*, 5222−5228.
(38) Kresse, G.; Hafner, J. Ab Initio Molecular Dynamics for Liquid Metals. *Phys. Rev. B* **1993**, *47*, 558−561.
(39) Kresse, G.; Hafner, J. Ab Initio Molecular-Dynamics Simulation of the Liquid-Metal−Amorphous-Semiconductor Transition in Germanium. *Phys. Rev. B* **1994**, *49*, 14251−14269.
(40) Kresse, G.; Furthmüller, J. Efficiency of Ab-Initio Total Energy Calculations for Metals and Semiconductors Using a Plane-Wave Basis Set. *Comput. Mater. Sci.* **1996**, *6*, 15−50.
(41) Kresse, G.; Furthmüller, J. Efficient Iterative Schemes for Ab Initio Total-Energy Calculations Using a Plane-Wave Basis Set. *Phys. Rev. B: Condens. Matter Mater. Phys.* **1996**, *54*, 11169−11186.
(42) Perdew, J. P.; Burke, K.; Ernzerhof, M. Generalized Gradient Approximation Made Simple. *Phys. Rev. Lett.* **1996**, *77*, 3865−3868.
(43) Heyd, J.; Scuseria, G. E.; Ernzerhof, M. Hybrid Functionals Based on a Screened Coulomb Potential. *J. Chem. Phys.* **2003**, *118*, 8207.
(44) Krukau, A. V.; Vydrov, O. A.; Izmaylov, A. F.; Scuseria, G. E. Influence of the Exchange Screening Parameter on the Performance of Screened Hybrid Functionals. *J. Chem. Phys.* **2006**, *125*, 224106.
(45) Kresse, G.; Joubert, D. From Ultrasoft Pseudopotentials to the Projector Augmented Wave Method. *Phys. Rev. B* **1999**, *59*, 1758−1775.
(46) Solovyev, I. V. Spin-Orbital Superexchange Physics Emerging from Interacting Oxygen Molecules in KO_2. *New J. Phys.* **2008**, *10*, 013035.
(47) Christensen, R.; Hummelshøj, J. S.; Hansen, H. A.; Vegge, T. Reducing Systematic Errors in Oxide Species with Density Functional Theory Calculations. *J. Phys. Chem. C* **2015**, *119*, 17596−17601.
(48) Garcia-Lastra, J. M.; Myrdal, J. S. G.; Christensen, R.; Thygesen, K. S.; Vegge, T. DFT+U Study of Polaronic Conduction in Li_2O_2 and Li_2CO_3: Implications for Li-Air Batteries. *J. Phys. Chem. C* **2013**, *117*, 5568−5577.
(49) Cococcioni, M.; de Gironcoli, S. Linear Response Approach to the Calculation of the Effective Interaction Parameters in the LDA+U Method. *Phys. Rev. B* **2005**, *71*, 35105.
(50) Larsen, A. H.; Mortensen, J. J.; Blomqvist, J.; Castelli, I. E.; Christensen, R.; Dułak, M.; Friis, J.; Groves, M. N.; Hammer, B.; Hargus, C.; et al. The Atomic Simulation Environment - A Python Library for Working with Atoms. *J. Phys. Condens. Matter* **2017**, *29*, 273002.
(51) Chase, M. W., Jr. *NIST-JANAF Thermochemical Tables*, 4th ed.; American Chemical Society: Woodbury, NY, 1998.
(52) Henkelman, G.; Uberuaga, B. P.; Jónsson, H. A Climbing Image Nudged Elastic Band Method for Finding Saddle Points and Minimum Energy Paths. *J. Chem. Phys.* **2000**, *113*, 9901.
(53) Radin, M. D. First-Principles and Continuum Modeling of Charge Transport in Li-O2 Batteries. P.D. dissertation, University of Michigan, Ann Arbor, MI, USA, 2014, http://hdl.handle.net/2027.42/110343.
(54) Gerbig, O. *Defect Chemistry in Alkali Peroxides and Superoxides*; Max-Planck-Institut für Festkörperforschung: Stuttgart, Germany, 2014.

DOI: 10.1021/acs.chemmater.9b03592
Chem. Mater. XXXX, XXX, XXX−XXX